Article

Hybrid PbS Quantum Dots/Nanoporous NiO Films Nanostructure: Preparation, Characterization, and Application for Novel Self-Powered Cathodic Photoelectrochemical Biosensor

Wen-Xia Dai, Ling Zhang, Wei-Wei Zhao, Xiao-Dong Yu, Jing-Juan Xu, and Hong-Yuan Chen

Anal. Chem., **Just Accepted Manuscript** • DOI: 10.1021/acs.analchem.7b01557 • Publication Date (Web): 06 Jul 2017

Hybrid PbS Quantum Dots/Nanoporous NiO Films Nanostructure: Preparation, Characterization, and Application for Novel Self-Powered Cathodic Photoelectrochemical Biosensor

Wen-Xia Dai,[†] Ling Zhang,[†] Wei-Wei Zhao,[,†,‡] Xiao-Dong Yu,[*,†] Jing-Juan Xu[†] and Hong-Yuan Chen[†]*

[†]State Key Laboratory of Analytical Chemistry for Life Science and Collaborative Innovation Center of Chemistry for Life Science, School of Chemistry and Chemical Engineering, Nanjing University, Nanjing 210023, China.

[‡]Department of Materials Science and Engineering, Stanford University, Stanford, California 94305, United States

* E-mail: zww@nju.edu.cn; zww@stanford.edu

* E-mail: yuxd@nju.edu.cn

Abstract: This work reports the first preparation and characterization of hybrid PbS quantum dots (QDs)/nanoporous NiO films nanostructure as well as its application for novel self-powered cathodic photoelectrochemical (PEC) sensing. Specifically, we synthesized the thioglycolic acid (TGA)-capped PbS QDs and then assembled it onto the hydrothermal-fabricated 3D NiO nanostructured films on the transparent indium tin oxide (ITO)-coated glass substrates, followed by the subsequent conjugation with the glucose oxidase (GOx) as a model biocatalyst. Favorable alignment existed between the NiO and PbS QDs, and the as-obtained p-type heterostructure was characterized by various techniques and found with good PEC activities. In the self-powered PEC biosensing of glucose, the system exhibited high sensitivity toward the presence of dissolved oxygen in the electrolyte and thereby a novel PEC enzymatic sensor was developed. With PbS QDs/3D NiO nanofilm, this work manifested the great promise of heterostructure photocathode for self-powered PEC biosensor which to our knowledge has not been reported. It is believed that it could inspire more interests in the design and development of numerous other p-type heterostructure for advanced self-powered PEC biosensor.

Keywords: Self-powered biosensor; Photoelectrochemistry; PbS; NiO; Glucose oxidase;

With the ever-growing demands for future sensing, there have been continuous efforts on exploiting novel techniques with ingenious signaling strategies.[1-4] Self-powered sensors, a rapidly developing concept, eliminate the common necessity of the external power sources and permit the detection without applying any voltage bias between the cathode and anode.[5,6] Such unique characteristic, along with the simple fabrication process, miniature size and low cost, make them as promising candidates in human disease diagnosis especially as battery-less portable devices.[7-11] Using semiconductors, self-powered photoelectrochemical (PEC) biosensor is a newly developed and promising method that offers good sensitivity, portability, and possibility of miniaturization and integration.[12-14] Currently, with the development of nanoscience and nanotechnology, more interest has been focused on the design and applications of functional semiconductor species for innovative self-powered PEC biosensor.[6,15-23] In the quest for achieving the desired performances and proper stability, judiciously designed heterostructures consisting of two semiconductors are being looked upon as favorite photoelectrode schemes.[24-30] Previous literature have also demonstrated different heterostructures as effective tool towards extending the absorbance to the visible region and improving photogenerated separation of charge carriers with increased lifetime.[31-34] However, consistently, appropriate band gap, proper band edge alignment with each other and with the redox potential of electron donor/acceptor, minimum lattice mismatch, high stability, and the ideal integration with the biorecognition events are the fundamental requirements for the construction of efficient PEC biosensor system.[35-39] To date, reported heterostructures for PEC biosensing have mainly focused on the coupling of various n-type TiO_2 species (nanoparticles (NPs), nanotubes (NTs) or nanowires (NWs) with n-type Cd-chalcogenide (S, Se, Te) quantum dots (QDs), leading to the developments of different photoanodes.[40,41] For self-powered PEC biosensing, significantly, Zhang et al. reported the self-powered sensing platform using $Ni(OH)_2/CdS/TiO_2$, hemin-graphene nanocomposite and glucose as the photoanode, the photocathode, and a model analyte, respectively.[22]

Different from n-type semiconductors with electrons as the major charge carriers responsible for their conductivity, p-type semiconductors have holes as the majority carriers.[42-45] As to their functions,

p-type ones operate in an inverse mode to that of n-type ones. Specifically, fast transfer of holes than that of electrons towards the electrolyte solution leads to the generation of anodic photocurrent (in n-type semiconductors), while faster electron transfer towards the electrolyte solution resulting into the flow of cathodic photocurrent (in p-type semiconductors).[46] In other words, in PEC bioanalysis, p-type semiconductors are prone to interact with electron acceptors (e.g., dissolved oxygen) more than electron donors (e.g., ascorbic acid) in the electrolyte, indicating their great capability in anti-interference from reductive substances.[47] Besides, semiconductors are found to be more resistant to reduction reactions than that of oxidation reactions, which makes p-type material more suitable than n-type material in terms of stability. In spite of their fascinating characteristics, the study in this domain is quite far behind. Recently, p-type BiOI and $CuInS_2$ were used to construct the cathodic PEC aptasensor[23] and cathodic PEC immunoassay,[21] respectively. As to the heterojunction photocathodes, at present, only limited work exploited the use of p-type species for the construction of p-n heterojunction comprised of e.g. p-type BiOI and n-type TiO_2 proposed by our group.[48,49] Obviously, novel p-type based heterostructures and their smooth application in efficient self-powered PEC bioanalysis is highly desirable.

NiO is a low-cost p-type large band gap (3.6–4.0 eV) semiconductor which mainly adsorbs ultraviolet light and can be easily fabricated by multiple methods.[50-52] Currently, sensitized NiO based photocathode is a new field of investigation with increasing scientific interest due to its high accessibility, balanced economics, and desired efficiency.[53,54] Especially, a three-dimensional (3D) nanoporous NiO structure with high specific surface area would be more advantageous for the loading of a large amount of sensitizers. On the other hand, PbS is an attractive narrow band gap (ca. 0.41 eV at 300 K) semiconductor and usually exists as a p-type semiconductor.[55] PbS possesses a large exciton Bohr radius, a high dielectric constant and carrier mobility, as well as strong confinement effects on charge carriers.[56,57] Significantly, PbS QD can exhibit the multiple exciton generation (MEG) effect, in which the excitation of PbS QDs by one high-energy photon can generate multiple electron−hole pairs.[58] Because of the reduction in the thermalization of those electron-hole pairs, enhanced energy conversion efficiency is expected with MEG effect. In addition, longer excited-state lifetimes (~2.6 μs)

are observed for PbS QDs as compared to those of extensively used n-type Cd-chalcogenide (e.g., CdS or CdSe QDs).[59] Inspired by their intriguing properties, of particular interest here is the possibility of integrating PbS QDs with the 3D porous NiO nanofilm to exploit the innovative heterostructure photocathode toward advanced PEC bioassay application. To our knowledge, such a heterostructure has seldom been constructed and studied, and its further application for cathodic PEC detection has also not been reported.

Scheme 1. Schematic Illustrations for (a) the Preparation of PbS QDs/3D NiO Porous Nanostructures and Its Application for the PEC Bioanalysis of Glucose and (b) the Operation Principle of the Proposed Sensor.

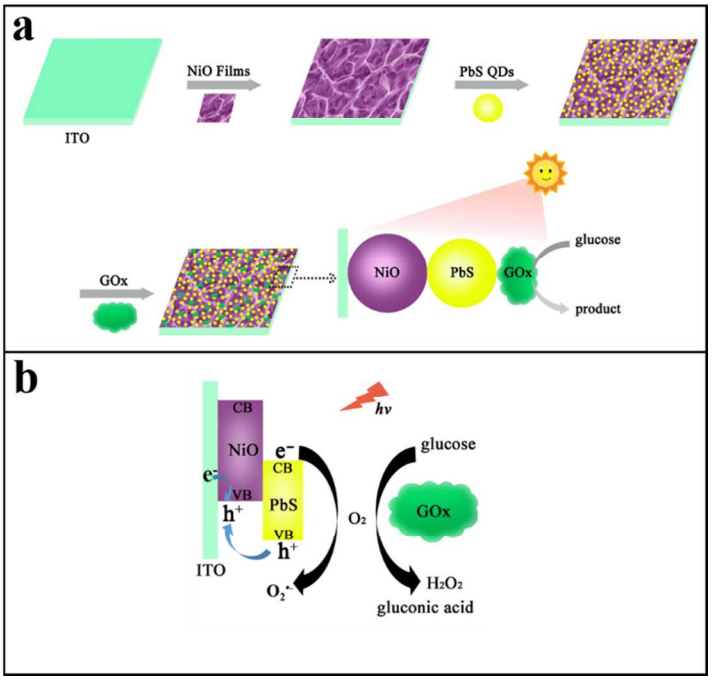

In this scenario, as shown in Scheme 1a, we demonstrate the self-powered PEC biosensor through the preparation and characterization of hybrid PbS QDs/3D nanoporous NiO film nanostructures and its application as an elegant photocathode for the highly efficient cathodic PEC detection. Specifically, we synthesized the thioglycolic acid (TGA)-capped PbS QDs and then assembled it onto the as-fabricated 3D NiO nanostructured films on the transparent indium tin oxide (ITO)-coated glass substrates, followed by the subsequent conjugation with the glucose oxidase (GOx) as a model biocatalyst via the classic N-(3-dimethylaminopropyl)-N-ethyl-carbodiimide hydrochloride (EDC) coupling reactions between the COOH groups on the surface of the TGA-capped PbS QDs and the NH_2 groups of the

biomolecules. In the PEC detection of glucose, the system was found very sensitive toward the presence of dissolved oxygen in the electrolyte and thereby a novel PEC enzymatic sensor could be developed. This work reported the first construction of a PbS QDs/3D NiO porous nanostructure and its exquisite utilization as a heterojunction photocathode for self-powered PEC biosensor. We expect it could inspire more interest in the design and development of numerous other advanced heterostructures for elegant self-powered PEC bioanalysis.

EXPERIMENTAL SECTION

Reagents and Apparatus. Thioglycolic acid (TGA), sodium sulfide nonahydrate, glucose oxidase (GOx, G2133-10 KU), dopamine (DA), N-(3-dimethylaminopropyl)-N-ethyl-carbodiimide hydrochloride (EDC), N-hydroxysuccinimide (NHS), hexamethylenetetramine, Poly(diallyldimethylammonium chloride) (PDDA, 20%, w/w in water, MW = 200 000-350 000) were supplied from Sigma-Aldrich, (St. Louis, MO). Nickel nitrate was supplied from Strem Chemicals, Inc. D-(+)-glucose, ascorbic acid (AA), urea, L-histidine, L-valine, L-lysine, L-leucine, L-proline, Tris (hydroxymethyl) aminomethane (Tris-HCl), Sodium hydroxide were supplied from Sinopharm Chemical Reagent Co., Ltd (China). Lead nitrate was supplied from Nanjing Chemical Reagent Co., Ltd. The indium tin oxide (ITO) glass (type N-STN-S1-10 with ITO coating 180±20 nm, sheet resistance 8.1± 0.6 Ω cm^{-2}) was obtained from China Southern Glass Holding Co., Ltd., Shenzhen, China.

Ultrapure water (18.2 MΩ·cm resistivity at 25 °C, Millier Q) was used in all experiments. Scanning electron microscope (SEM) images were recorded by a Hitachi S4800 scanning electron microscope (Hitachi Co., Japan). Transmission electron microscope (TEM) was performed with a JEM-2100 microscope (JEOL, Japan). X-ray photoelectron spectroscopy (XPS) was obtained from PHI 5000 VersaProbe (UlVAC-PHI Co., Japan). The UV-vis absorption spectra and UV−vis diffuse reflectance spectra were obtained on a Shimadzu UV-3600 UV-vis-NIR spectrophotometer (Shimadzu Co., Japan). XRD spectra were characterized by powder X-ray diffraction (XRD, X'TRA, Cu Kα; ARL Co., Switzerland).

PEC measurements were performed with a homemade PEC system equipped with a 5 W LED lamp emitting at around 415 nm with a power density of 1.6 mW cm^{-2}. Photocurrent was measured on a CHI 660C electrochemical workstation with a three-electrode system: a PbS/NiO/ITO electrode with a geometrical circular area (0.5 cm in diameter) as the working electrode, a Pt wire as the counter electrode and a saturated Ag/AgCl electrode as the reference electrode. The photocurrent measurements were performed at a constant potential of 0.0 V (vs saturated Ag/AgCl). A 0.1 M Tris–HCl (pH 7.0) was used as the supporting electrolyte for photocurrent measurements.

Synthesis of TGA-stabilized PbS QDs: The utilized PbS QDs was synthesized according to the previous report with a slight modification.[60] 34 μL of TGA was added to 50 mL of 4.0 mM $Pb(NO_3)_2$ aqueous solution, followed by addition of 1.0 M NaOH to adjust the mixed solution to the desired value of pH 11. N_2 was bubbled throughout the solution to remove O_2 for 30 min. Then, 4.0 mL of 0.015 M Na_2S aqueous solution was injected and the reaction mixture was stirred under N_2 atmosphere for 4 h. The as-synthesized TGA-capped PbS QDs were stored at 4 °C.

Synthesis of nanoporous 3D NiO modified ITO electrodes: NiO nanofilm was fabricated on ITO glass substrates using the hydrothermal method.[52] The ITO slices were cleaned by immersion in 2.0 M boiling KOH solution solved in 2-propanol for 20 min, followed by washing copiously with water and dried at 80 °C. Then the ITO slices were cleaned by piranha solution, followed by washing thoroughly with ultrapure water and dried at 80 °C. For the hydrothermal method, the reaction solution was aqueous, containing 0.25 M $Ni(NO_3)_2 \cdot 6H_2O$ and 0.25 M $C_6H_{12}N_4$. The above solution was transferred into a vial and the ITO electrodes were placed at the bottom of the vial. The vial was then heated in an oven at 90 °C for 10 min. Then the ITO was washed with ultrapure water for about 10 times, dried and heated to 300 °C in air for 30 min.

Fabrication of PbS QDs/3D NiO Modified ITO Electrode: The NiO modified ITO electrode was dipped into PDDA (2% PDDA, 0.5 M NaCl, pH = 8) aqueous solution for 10 min, washed with ultrapure water. Then, the electrode was immersed into the as-fabricated PbS QDs solution for 10 min.

Repeating process was done by dipping into PDDA and PbS QDs solutions in order to obtain multilayers of NiO/PbS QDs modified electrodes.

Biosensor Development: GOx was bioconjugated onto the PbS QDs/3D NiO modified ITO electrode via the classic succinimide coupling (EDC-NHS) reaction between COOH groups on the surface of the TGA-capped PbS QDs and the NH_2 groups of GOx.[61] The electrode was dipped into the solution containing 20 mg mL^{-1} EDC and 10 mg mL^{-1} NHS for 1 h at room temperature, followed by thoroughly rinsing with washing buffer. Then, 25 μL 0.5 mg mL^{-1} GOx was spread onto the resulting electrode surface at 4 ºC for 14 h, followed by rinsing with the washing buffer to remove physically adsorbed GOx. For glucose detection, the NiO/PbS/GOx electrode was immersed in 7 mL 0.1 M Tris–HCl buffer (pH 7.0, containing certain concentration of glucose) at 35 ºC. 10 minutes later, the photocurrent of the NiO/PbS/GOx electrode was measured. To detect glucose in real samples, 70 μL glucose injection (the sample was obtained from Nanjing University Hospital) was added to 7 mL 0.1 mol L^{-1} Tris–HCl buffer (pH 7.0) for photocurrent measurements.

RESULTS AND DISCUSSION

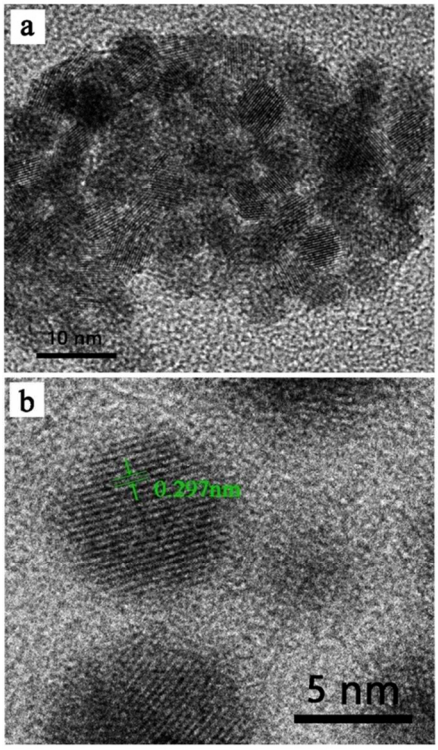

Fig. 1. (a) TEM and (b) HRTEM of the as-synthesized PbS QDs.

Structural Characterization. TEM, SEM and XRD were utilized to reveal the structural information of the samples. Figure 1a shows the TEM image of the as synthesized TGA-capped PbS QDs, which appeared as quasi-spherical particles with the sizes corresponding to c.a. 6 nm. The HRTEM image of individual QDs, as shown in Figure 1b, implied that they had relatively good crystallization, and the lattice spacing of ~0.297 nm was observed, corresponding to the (200) plane of cubic PbS. The morphology of NiO nanofilm was then revealed by SEM with the image shown in Figure 2a. Obviously, the as-fabricated nanostructured NiO thin film exhibited a highly crossed three-dimensional (3D) porous architecture that composed of densely interconnected nanosheets. The high-magnification SEM image of Figure 2b revealed these nanosheets have lateral dimension in the micrometer size, average thickness of ca. 10 nm, and height of several hundred nm. The accurate height of the film, as shown in Figure 2b inset, was then determined as ca. 500–600 nm by the cross-sectional view. Such a porous 3D nanostructure could provide great surface area for the subsequent loading of guest species PbS QDs and also be advantageous to the efficient charge separation and transfer of the photogenerated electron-hole pairs. Figure 2c then reflected the morphology of hybrid PbS QDs/NiO nanofilm. Apparently, the smooth surface of NiO nanosheets exhibited an obvious roughness, which was easily attributed to the coating of numerous small PbS QDs. Figure 2d of the elemental mapping further verified the successful modification of PbS QDs onto these NiO nanosheets.

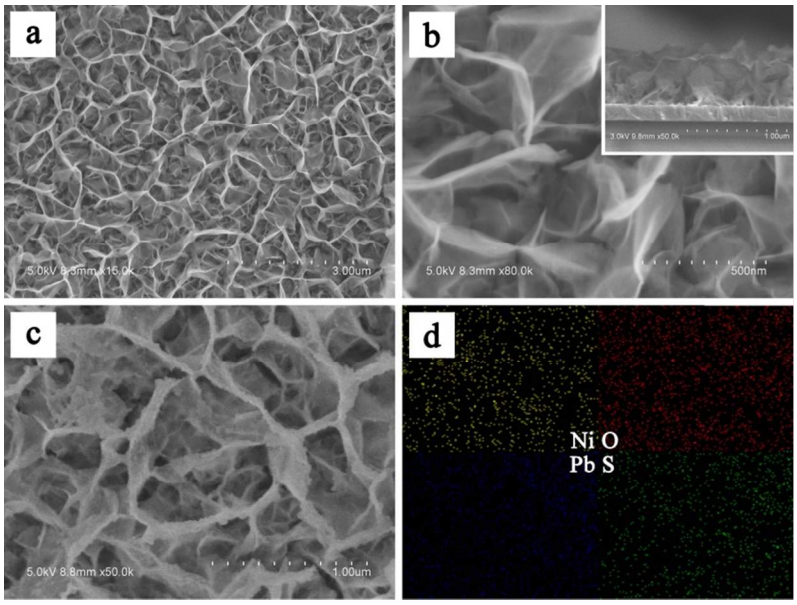

Fig. 2. (a) SEM and (b) HRSEM of the NiO nanofilm. Inset: the cross-sectional view. (c) SEM and (d) elemental mapping of the hybrid PbS QDs/NiO nanofilm.

The crystal structure of the as-fabricated PbS QDs, as-deposited NiO nanofilm and the hybrid PbS QDs/NiO nanofilm were further identified by XRD with the results shown in Figure 3. The XRD pattern of the PbS QDs possessed sharp diffraction peaks at scattering angles (2θ) of 25.94°, 30.02°, 43.02°, 50.86°, 53.44°, 62.38°, 68.80°, 71.02°, and 78.84°, corresponding to scattering from the (111), (200), (220), (311), (222), (400), (331), (420), and (422) planes of the standard cubic PbS [JCPDS:5-592]. This pattern indicated that the sample was face-centered cubic PbS. On the other hand, quantitative analysis of the pattern of NiO nanofilm would index all the observed peaks to the face-centered cubic NiO (JCPDS:78-0643), with characteristic peaks of the NiO at 2θ = 37.26°, 43.28°, 62.76°, 75.28° corresponding to the (111), (200), (220) and (311) crystal planes of cubic NiO, respectively. This implied that no Ni related impurities exist in the sample. Besides, the prominent and sharp peaks also indicated the sample had a relatively good crystallinity. As to the pattern of the PbS QDs/NiO nanofilm, both the peaks of pure PbS and NiO were observed, suggesting the successful integration of the two species.

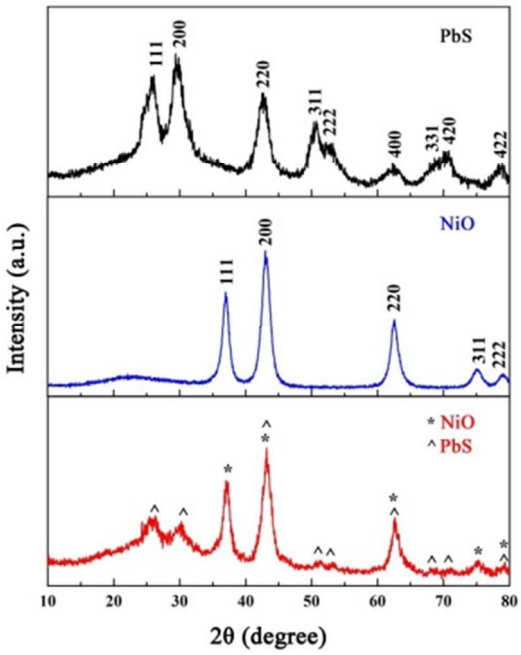

Fig. 3. XRD patterns of the as-fabricated PbS QDs, NiO nanofilm, and the PbS QDs/NiO nanofilm.

Compositional Characterization. XPS was further performed to study the surface chemical compositions and oxidation states of the PbS QDs/NiO nanofilm hybrid. The peak positions were determined with binding energy C 1s = 284.6 eV as the internal marked standard. Figure 4a depicts the full-scan XPS spectrum of the as-fabricated PbS QDs/NiO nanofilm with the relevant elements of Pb, S, Ni, O and C. The corresponding high-resolution XPS spectra of Pb 4f, S 2p, Ni 2p and O 1s were also illustrated. Figure 4b presents the Pb $4f_{7/2}$ and Pb $4f_{5/2}$ signal with maximum located at about 137 eV and 141 eV, while Figure 4c shows the S 2p consisted of S $2p_{1/2}$ and S $2p_{3/2}$ at around 160 eV, which should be assigned to the PbS compound. Figure 4d of the Ni 2p exhibits several peaks in the range of 850 to 880 eV. Specifically, the peaks centered at ca. 853, 855, and 860 eV were attributed to Ni $2p_{3/2}$, while the peaks located at ca. 872 and 878 eV corresponded to Ni $2p_{1/2}$. Figure 4e of the O 1s spectrum exhibits two peaks at binding energies of ca. 528 and 530 eV. The peaks at 528 eV can be assigned to bridging O in NiO crystals, while the peak at higher binding energy can be ascribed to O^{2-} inoctahedral symmetry (bulk O) associated with NiO species. Figure 4f records the peak for C 1s, which was ascribed to the adventitious hydrocarbon from the instrument.

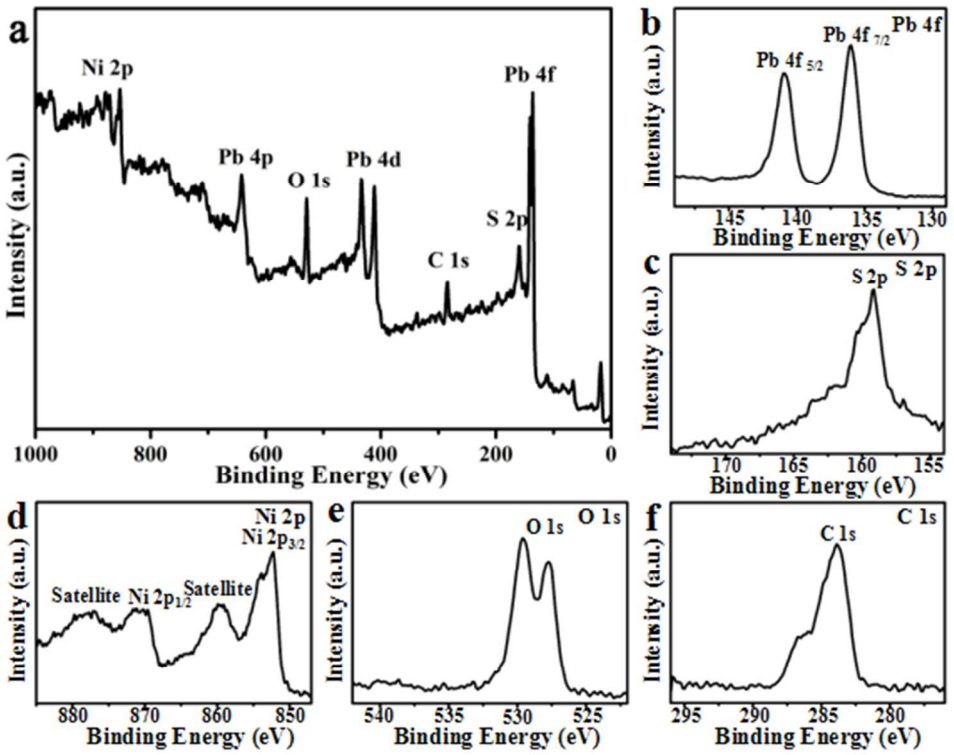

Fig. 4. (a) The full-scan XPS spectrum of the as-fabricated PbS QDs/NiO nanofilm, and (b-f) high-resolution XPS spectra of Pb 4f, S 2p, Ni 2p, O 1s and C 1s.

Optical Characterization. UV-vis absorption or diffuse reflectance spectra were also measured for PbS (black curve), NiO (red curve) and hybrid (blue curve) as shown in Figure 5a. Clearly, the bare NiO electrode hardly had any absorption for visible light due to its broad band gap excitation, while obvious absorption was monitored above 400 nm for PbS QDs. For PbS QDs/NiO nanofilm, enhanced absorption could be seen in the same range due to the attachment of sensitization of PbS QDs to NiO film. Especially, the consecutive rise of absorption further indicated its suitability to be a photoactive electrode under visible light irradiation. Incidentally, the photocurrent responses of the NiO and PbS QDs/NiO electrodes at different wavelengths were also examined with the expected results shown in Figure 5b.

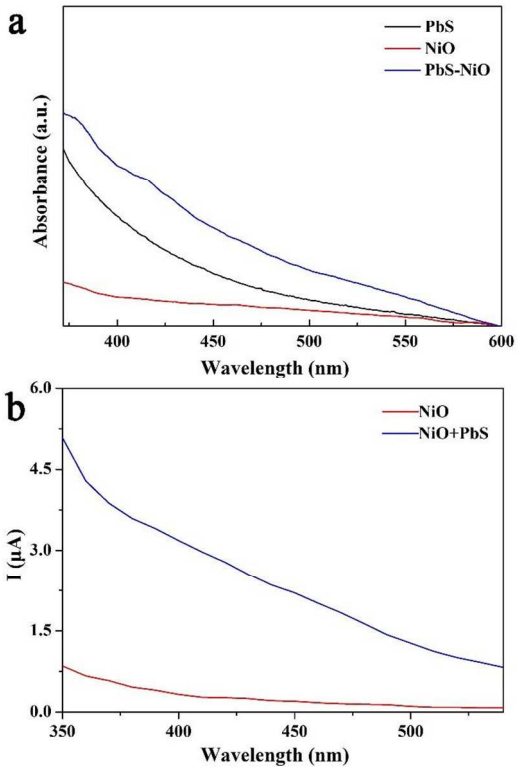

Fig. 5. (a) UV-vis absorption or diffuse reflectance spectra of PbS (black curve), NiO (red curve) and hybrid (blue curve). (b) Photocurrent response of NiO (red) and hybrid (blue curve) modified electrode at different wavelengths.

PEC Characterization. To obtain more enriched information on the light-harvesting properties of the samples, their PEC performances were then investigated and the results further confirmed the aforementioned measurements. The visible-light-responsibilities were first probed by photocurrent action spectra, and Figure 6a records the measured chronoamperometric I-t responses of NiO electrode (dark curve) and PbS QDs/NiO electrode (red curve) upon visible light illumination. As shown, upon irradiation, NiO/ITO electrode showed a very small cathodic photocurrent, whereas the PbS QDs/NiO exhibited much enhanced cathodic photocurrent under no biased potential, suggesting the successful coupling of PbS QDs and NiO nanofilm and thereby the excellent sensitization effect. To further study the feasibility of the proposed biosensor, the photocurrent response of the GOx/PbS QDs/NiO nanofilm in presence of glucose was also recorded (blue curve). Significantly, the signal exhibited great reduction as compared to that of PbS QDs/NiO nanofilm. Such a remarkable behavior, as proposed in Scheme 1b,

should be attributed to the following reasons: (1) The PbS QDs, with broad visible light absorption and efficient charge transport properties, could act as the excellent light-sensitive and charge-generating elements in the hierarchical system, while the porous nanoflake morphology of the NiO nanofilm could provide high specific area for PbS loading and effectively accelerate the electron transport between PbS QDs and NiO. (2) Upon illumination, the fast charge excitation, separation and transfer process would occur within the system. Namely, the photogenerated electrons would rapidly transfer from the conduction band (CB) of PbS QDs to the electron acceptors (i.e. the dissolved oxygen) in the electrolyte, while the photogenerated holes would transfer to the valence band (VB) of NiO and then easily be captured by the ITO electrode to generate the cathodic photocurrent. (3) When coupled with GOx, the enzymatic catalysis would quickly consume the ambient oxygen, the event of which could compete greatly with the aforementioned photogenerated electrons transfer process and thus inhibit the photocurrent generation. The stability of the photocurrent response of the as-fabricated PbS QDs/NiO nanofilm/ITO electrode was also studied as shown in Figure 6b. For this photocathode, as shown, the photocurrent intensity did not show any obvious decay under continuous illumination in 300s. Figure 6b inset reveals the operational stability by recording with 15 repeated on/off illumination cycles over 5 min, and the electrode displayed reproducible responses without any noticeable decrease during this period. These results indicated the high mechanical and photophysical stability of the electrode in PEC measurements. Besides, upon the onset/offset of irradiation, the rapid rise and fall of the signals also suggested the excellent electrical contact between the crossed NiO and the ITO substrate due to the hydrothermal fabrication, and thus the efficient charge collection as photocurrent signal.

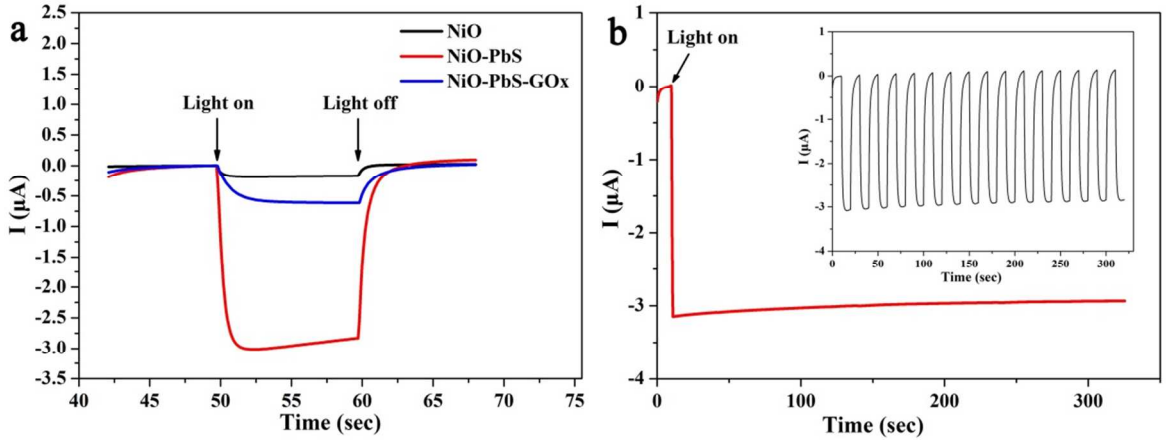

Fig. 6. (a) Photocurrent responses of NiO nanofilm/ITO (dark curve), PbS QDs/NiO nanofilm/ITO (red curve) and GOx/PbS QDs/NiO nanofilm/ITO (blue curve) corresponding to 1.0×10^{-6} M glucose in air saturated 0.1 M Tris–HCl solution (pH=7.0) at 0 V vs. Ag/AgCl under visible light irradiation. (b) Time-based photocurrent response of the photocurrent response of the as-fabricated PbS QDs/NiO nanofilm/ITO electrode. Inset: the operational stability test by repeated on/off illumination cycles.

Besides, the sensitivity of this photocathode to the ambient oxygen was further investigated. As shown in the Figure 7a, if the air-saturated electrolyte was deoxygenated by purging with highly pure nitrogen, a total inhibition of the cathodic photocurrent could be produced (red curve). Since the GOx can oxidize glucose by the reduction of dissolved O_2 to generate gluconic acid and H_2O_2, 1.0×10^{-3} M H_2O_2 was further added in the electrolyte and no obvious influence was found (blue curve). Previous reports have also demonstrated dissolved O_2 were much more influential than H_2O_2 in both PEC and electrochemiluminescent systems.[62] Further research, as shown in Figure 7a inset, indicated the cathodic photocurrent of the hybrid electrode could be reversibly generated/inhibited by the on/off state of dissolved O_2 in the electrolyte solution, implying the important role of oxygen as an electron acceptor against the photocurrent generation of the photocathode. Incidentally, the I-V characteristic curves of hybrid electrode were also measured upon illumination (solid line) and in the dark (dashed line) with the results shown in Figure 6b. Both the two curves increased as the applied potential increased from -0.2 to +0.2 V, in all of the range the photocurrent density was higher than that in dark, indicating the PEC effect for enhancing the cathodic photocurrent generation. Obviously, light illumination would allow the operation of the proposed self-powered system.

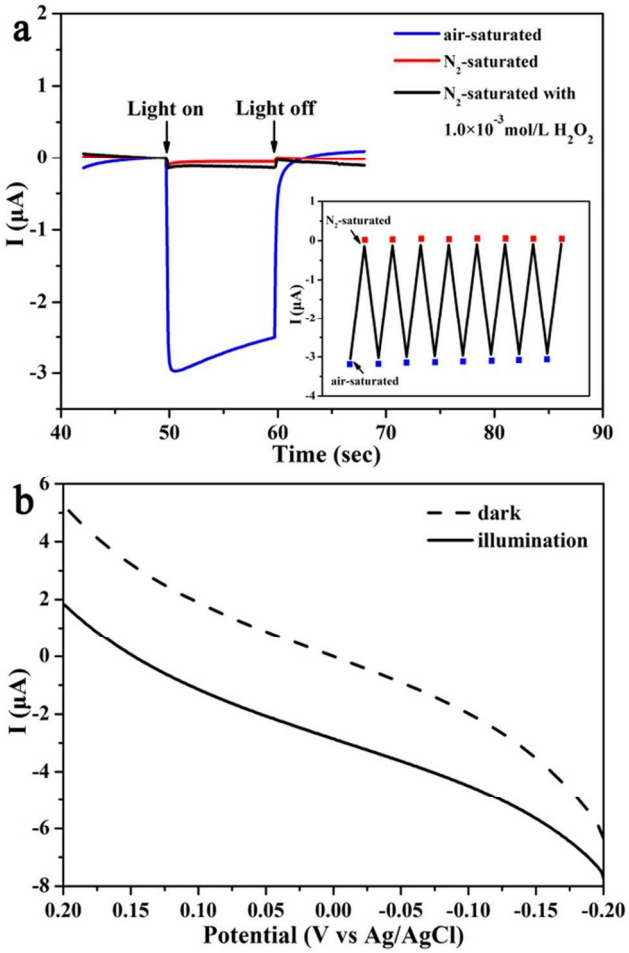

Fig. 7. (a) Photocurrent responses of PbS QDs/NiO nanofilm in aerated (black curve), deaerated 0.1 M Tris–HCl solution (pH=7.0) before (red curve) and after (blue) the addition of 1.0×10^{-3} M H_2O_2, at 0 V vs. Ag/AgCl under visible light irradiation. Inset: Photocurrent responses of the electrode during consecutive O_2 ON and OFF state. (b) I–V characteristic curves of the electrode upon illumination (solid line) and in the dark (dashed line) with the range of -0.2 to +0.2 V.

Analytical Performance. We then implemented the developed PbS QDs/NiO nanofilm photocathode along with the GOx catalytic events for model glucose determination. Figure 8a demonstrated the photocurrent responses in the presence of variable glucose concentration at a bias potential of 0.0 V. The cathodic photocurrent decreased steadily with the increased glucose concentration, and reached a saturation level at c.a. 1.0×10^{-2} M glucose concentration. This negative correlation between the observed cathodic photocurrent and glucose concentration was caused by the competition of the photocathode and GOx toward the dissolved O_2. As aforementioned, when the GOx immobilized

electrode was exposed to a solution containing glucose, the GOx could efficiently catalyze the conversion of glucose into gluconic acid and hydrogen peroxide with the rapid consumption of dissolved oxygen, thus inhibiting the photoinduced electron transfer and depressing the cathodic photocurrent. Figure 8a inset depicted the corresponding derived calibration curve. Significantly, wide linear range of 1.0×10^{-6} M-1.0×10^{-2} M and low detection limit of 3.0×10^{-7} M were experimentally obtained, which were superior to previous glucose detections.[63-66] Reproducibility of this system was assessed by an interassay relative standard deviation (RSD) through testing 1.0×10^{-3} mM samples with five electrodes, and RSD of 5.7% was calculated, suggesting the good reproducibility. As aforementioned, the photocathodes have good anti-interference ability (enhanced selectivity) against the reductive agents coexisting in biological samples and hence has large potential in PEC biosensing. The selectivity of the proposed self-powered sensor was then evaluated with the results shown in Figure 8b. The common co-existing interfering species such as ascorbic acid (AA), uric acid (UA), dopamine (DA), and few of the amino acid were examined. Although the normal physiological glucose level in the human blood is 3-8 mM, which is nearly 30 times higher than many of the interfering species, the interference experiments in this work were carried out by using glucose and interfering species at the same concentration of 1.0 mM. Clearly, except the glucose, all of these species could not cause any influence, revealing the excellent selectivity of this self-powered detection system. As a proof of principle, these results demonstrated the great potential of the proposed hybrid system for the development of sensitive self-powered PEC enzymatic biosensor. The feasibility of the proposed system for practical application was evaluated by a recovery experiment conducted in the real sample of glucose injections. The sample was diluted to specific concentration with a Tris-HCl (pH 7.0), and recovery of the 2 mM and 10 mM glucose was determined as 97.47 ± 5.4% and 95.93 ± 6.8%, respectively, indicating the applicability of the proposed system for future utilization.

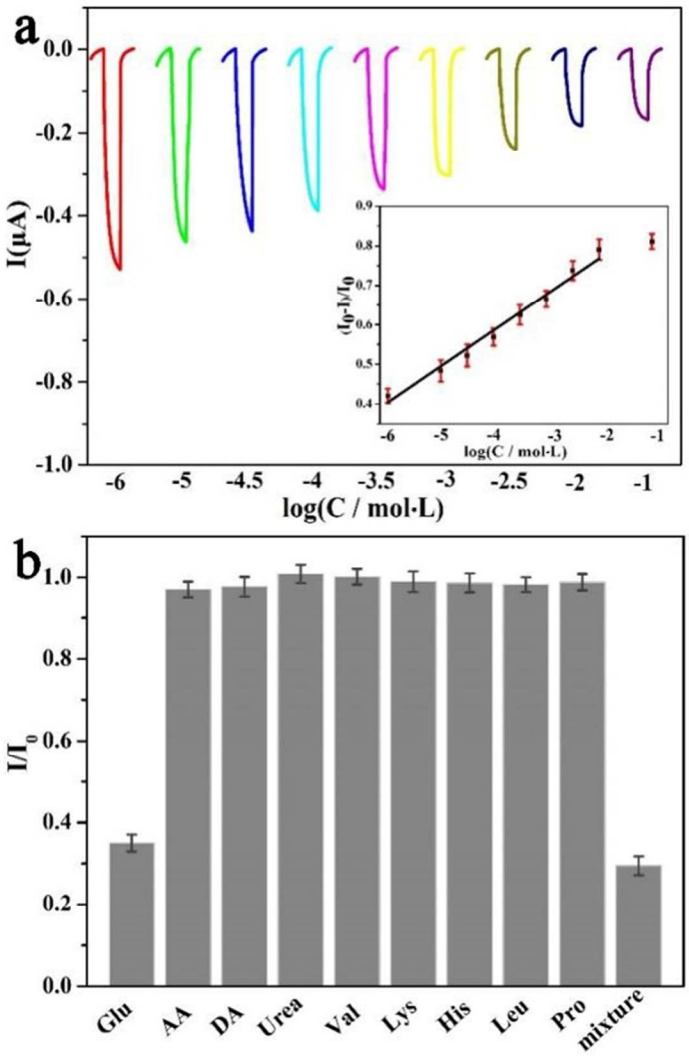

Fig. 8. (a) Photocurrent responses of the enzyme electrode corresponding to different glucose concentrations. Inset: Plot of photocurrent decrease (I_0-I/I_0) of GOx modified electrode versus minus logarithm $C_{glucose}$. I_0 and I were the photocurrent of GOx modified electrode before and after reaction with glucose, respectively. (b) Effect of different substance (1.0×10^{-3} M): glucose, ascorbic acid (AA), dopamine (DA), urea, L-Valine (Val), L-Lysine (Lys), L-Histidine (His), L-Leucine (Leu), L-Proline (Pro) on the photocurrent intensity of ITO/NiO/PbS/GOx electrode.

CONCLUSIONS

In conclusion, this work has demonstrated the construction and characterization of p-type hybrid PbS QDs/NiO nanofilm nanostructure and its utilization as a novel photocathode for the self-powered cathodic PEC bioanalysis. The structure and composition characterization demonstrated the ideal coupling of PbS QDs onto the NiO nanofilm with excellent properties. Due to the favorable

sensitization effect, the as-obtained heterostructure possessed superior PEC activities and oxygen sensitivity as revealed by the chronoamperometric I-t tests. For the model detection of glucose, the biosensor exhibited good analytical performance in terms of high sensitivity, excellent selectivity, rapid response and high stability. This work manifested the great promise of heterostructure photocathode for self-powered PEC biosensor. More generally, we believed this work could inspire more interest in the design and development of numerous other heterostructure for advanced self-powered PEC biosensing of numerous other targets of interest.

ASSOCIATED CONTENT

AUTHOR INFORMATION

Corresponding Authors

* E-mail: zww@nju.edu.cn; zww@stanford.edu

* E-mail: yuxd@nju.edu.cn

Notes

The authors declare no competing financial interest.

ACKNOWLEDGMENT

We thank the National Natural Science Foundation of China (Grant Nos. 21327902, 21305063, and 21675080) for support. This work was also supported by a Project Funded by the Priority Academic Program Development of Jiangsu Higher Education Institutions.

REFERENCES

(1) Dou, Z. S.; Yu, J. C.; Cui, Y. J.; Yang, Y.; Wang, Z. Y.; Yang, D. R.; Qian, G. D. *J. Am.Chem. Soc.* **2014**, *136*, 5527.

(2) Li, Y. H.; Luo, W.; Qin, N.; Dong, J. P.; Wei, J.; Li, W.; Feng, S. S.; Chen, J. C.; Xu, J. Q.; Elzatahry, A. A.; Es-Saheb, M. H.; Deng, Y. H.; Zhao, D. Y. *Angew. Chem. Int. Ed.* **2014**, *53*, 9035.

(3) Maiti, S.; Pezzato, C.; Martin, S. G.; Prins, L. J. *J. Am. Chem. Soc.* **2014**, *136*, 11288.

(4) Xu, J. Q.; Liu, Y. L.; Wang, Q.; Duo, H. H.; Zhang, X. W.; Li, Y. T.; Huang, W. H. *Angew. Chem. Int. Ed.* **2015**, *54*, 14402.

(5) Zhao, W. W.; Xu, J. J.; Chen, H. Y. *Chem. Soc. Rev*. **2015**, *44*, 729.

(6) Kang, Z.; Yan, X. Q.; Wang, Y. F.; Zhao, Y. G.; Bai, Z. M.; Liu, Y. C.; Zhao, K.; Cao, S. Y.; Zhang, Y. *Nano Res*. **2016**, *9*, 344.

(7) Zhu, Y. C.; Zhang, N.; Ruan, Y. F.; Zhao, W. W.; Xu, J. J.; Chen, H. Y. *Anal. Chem*. **2016**, *88*, 5626.

(8) Haddour, N.; Chauvin, J.; Gondran, C.; Cosnier, S. *J. Am.Chem. Soc.* **2006**, *128*, 9693.

(9) Ma, Z. Y.; Xu, F.; Qin, Y.; Zhao, W. W.; Xu, J. J.; Chen, H. Y. *Anal. Chem.* **2016**, *88*, 4183.

(10) Long, Y. T.; Kong, C.; Li, D. W.; Li, Y.; Chowdhury, S.; Tian, H. *Small* **2011**, *7*, 1624.

(11) Zhao, W. W.; Han, Y. M.; Zhu, Y. C.; Zhang, N.; Xu, J. J.; Chen, H. Y. *Anal. Chem*. **2015**, *87*, 5496.

(12) Kang, Z.; Yan, X. Q.; Wang, Y. F.; Bai, Z. M.; Liu, Y. C.; Zhang, Z.; Lin, P.; Zhang, X. H.; Yuan, H. G.; Zhang, X. J.; Zhang, Y. *Sci. Rep.* **2015**, *5*, 7882.

(13) Bellani, S.; Ghadirzadeh, A.; Meda, L.; Savoini, A.; Tacca, A.; Marra, G.; Meira, R.; Morgado, J.; Fonzo, F. D.; Antognazza, M. R. *Adv. Funct. Mater.* **2015**, *25*, 4531.

(14) Li, X. D.; Gao, C. T.; Duan, H. G.; Lu, B. G.; Wang, Y. Q.; Chen, L. L.; Zhang, Z. X.; Pan, X. J.; Xie, E. Q. *Small* **2013**, *9*, 2005.

(15) Ma, Z. Y.; Ruan, Y. F.; Xu, F.; Zhao, W. W.; Xu, J. J.; Chen, H. Y. *Anal. Chem*. **2016**, *88*, 3864.

(16) Tang, J.; Kong, B.; Wang, Y. C; Xu, M.; Wang, Y. L.; Wu, H.; Zheng, G. F. *Nano Lett*. **2013**, *13*, 5350.

(17) Lee, C. Y.; Park, H. S.; Fontecilla-Camps, J. C.; Reisner, E. *Angew. Chem. Int. Ed*. **2016**, *55*, 5971.

(18) Fan, L. F.; Zhao, G. H.; Shi, H. J.; Liu, M. C.; Wang, Y. B.; Ke, H. Y. *Environ. Sci. Technol.* **2014**, *48*, 5754.

(19) Kong, B.; Sikdar, D.; Tang, J.; Liu, Y.; Premaratne, M.; Zhang, W.; Jing, Y. K.; Zheng, G. F.; Selomulya, C.; Zhao, D. Y. *NPG Asia Mater*. **2015**, *7*, e204.

(20) Zhao, W. W.; Xu, J. J.; Chen, H. Y. *Analyst* **2016**, *141*, 4262.

(21) Fan, G. C.; Shi, X. M.; Zhang, J. R.; Zhu, J. J. *Anal. Chem.* **2016**, *88*, 10352.

(22) Yan, K.; Yang, Y. H.; Okoth, O. K.; Cheng, L.; Zhang, J. D. *Anal. Chem.* **2016**, *88*, 6140.

(23) Yan, K.; Liu, Y.; Yang, Y. H.; Zhang, J. D. *Anal. Chem.* **2015**, *87*, 12215.

(24) Zhao, K.; Yan, X. Q.; Gu, Y. S.; Kang, Z.; Bai, Z. M.; Cao, S. Y.; Liu, Y. C.; Zhang, X. H.; Zhang, Y. *Small* **2016**, *12*, 245.

(25) Xiao, F. X.; Zeng, Z. P.; Liu, B. *J. Am. Chem. Soc.* **2015**, *137*, 10735.

(26) Tang, J.; Zhang. Y. Y.; Kong, B.; Wang, Y. C.; Da, P. M.; Li, J.; Elzatahry, A. A.; Zhao, D. Y.; Gong, X. G.; Zheng, G. F. *Nano Lett.* **2014**, *14*, 2702.

(27) Zhan, W. W.; Kuang, Q.; Zhou, J. Z.; Kong, X. J.; Xie, Z. X.; Zheng, L. S. *J. Am. Chem. Soc*. **2013**, *135*, 1926.

(28) Li, H. B.; Li, J.; Xu, Q.; Hu, X. Y. *Anal. Chem.* **2015**, *83*, 9681.

(29) Zayats, M.; Kharitonov, A. B.; Pogorelova, S. P.; Lioubashevski, O.; Katz, E.; Willner, I. *J. Am.Chem. Soc.* **2003**, *125*, 16006.

(30) Zhang, N.; Zhang, L.; Ruan, Y. F.; Zhao, W. W.; Xu, J. J.; Chen, H. Y. *Biosens. Bioelectron.* **2017**, *94*, 207.

(31) Li, H. N.; Mu, Y. W.; Yan, J. R.; Cui, D. M.; Ou, W. J.; Wan, Y. K.; Liu, S. Q. *Anal. Chem*. **2015**, *87*, 2007.

(32) Wang, H. L.; Zhang, L. S.; Chen, Z. G.; Hu, J. Q.; Li, S. J.; Wang, Z. H.; Liu, J. S.; Wang, X. C. *Chem. Soc. Rev.* **2014**, *43*, 5234.

(33) Zhao, W. W.; Yu, X. D.; Xu, J. J.; Chen, H. Y. *Nanoscale* **2016**, *8*, 17407.

(34) Li, H. P.; Liu, J. Y.; Hou, W. G.; Du, N.; Zhang, R. J.; Tao, X. T. *Appl. Catal. B* **2014**, 160-161, 89.

(35) Khalid, W.; Helou, M. E.; Murbock, T.; Yue, Z.; Montenegro, J. M.; Schubert, K.; Gobel, G.; Lisdat, F.; Witte, G.; Parak, W. J. *ACS Nano* **2011**, *5*, 9870.

(36) Zhuang, J. Y.; Lai, W. Q.; Xu, M. D.; Zhou, Q.; Tang, D. P. *Appl. Mater. Interfaces* **2015**, *7*, 8330.

(37) Zhang, B. T.; Guo, L. H. *Biosens. Bioelectron.* **2012**, *37*, 112.

(38) Chen, D.; Zhang, H.; Li, X.; Li, J. H. *Anal. Chem.* **2010**, *82*, 2253.

(39) Xiao, F. X.; Miao, J. W.; Liu, B. *J. Am. Chem. Soc.* **2014**, *136*, 1559.

(40) Zhao, W. W.; Xu, J. J.; Chen, H. Y. *Trends Anal. Chem.* **2016**, *82*, 307.

(41) Zhang, N.; Ma, Z. Y.; Ruan, Y. F.; Zhao, W. W.; Xu, J. J.; Chen, H. Y. *Anal. Chem*. **2016**, *88*, 1990.

(42) Gao, J. K.; Miao, J. W.; Li, P. Z.; Teng, W. Y.; Yang, L.; Zhao, Y. L.; Liu, B.; Zhang, Q. C. *Chem. Commun.* **2014**, *50*, 3786.

(43) Ning, Z. J.; Voznyy, O.; Pan, J.; Hoogland, S.; Adinolfi, V.; Xu, J. X.; Li, M.; Kirmani, A. R.; Sun, J. P.; Minor, J.; Kemp, K. W.; Dong, H. P.; Rollny, L.; Labelle1, A.; Carey, G.; Sutherland, B.; Hill, I.; Amassian, A.; Liu, H.; Tang, J.; Bakr, O. M.; Sargent, E. H. *Nat. Mater*. **2014**, *13*, 822.

(44) Chuang, S.; Battaglia, C.; Azcatl, A.; McDonnell, S.; Kang, J. S.; Yin, X. T.; Tosun, M.; Kapadia, R.; Fang, H.; Wallace, R. M.; Javey, A. *Nano Lett.* **2014**, *14*, 1337.

(45) Kibria, M. G.; Chowdhury, F. A.; Zhao, S.; AlOtaibi, B.; Trudeau, M. L.; Guo, H.; Mi, Z. *Nat. Commun*. **2015**, *6*, 6797.

(46) Zhao, W. W.; Xu, J. J.; Chen, H. Y. *Chem. Rev.* **2014**, *114*, 7421.

(47) Wang, G. L.; Shu, J. X.; Dong, Y. M.; Wu, X. M.; Zhao, W. W.; Xu, J. J.; Chen, H. Y. *Anal. Chem.* **2015**, *87*, 2892.

(48) Zhao, W. W.; Shan, S.; Ma, Z. Y.; Wan, L. N.; Xu, J. J.; Chen, H. Y. *Anal. Chem*. **2013**, *85*, 11686.

(49) Zhao, W. W.; Liu, Z.; Shan, S.; Zhang, W. W.; Wang, J.; Ma, Z. Y.; Xu, J. J.; Chen, H. Y. *Sci. Rep*. **2014**, *4*, 4426.

(50) Zhang, Y. Q.; Xia, X. H.; Tu, J. P.; Mai, Y. J.; Shi, S. J.; Wang, X. L.; Gu, C. D. *J. Power Sources* **2012**, *199*, 413.

(51) Xia, X. H.; Tu, J. P.; Wang, X. L.; Gu, C. D.; Zhao, X. B. *J. Mater. Chem.* **2011**, *21*, 671.

(52) Lepleux, L.; Chavillon, B.; Pellegrin, Y.; Blart, E.; Cario, L.; Jobic, S.; Odobel, F. *Inorg. Chem.* **2009**, *48*, 8245.

(53) Park, J. H.; Seo, J.; Park, S.; Shin, S. S.; Kim, Y. C.; Jeon, N. J.; Shin, H. W.; Ahn, T. K.; Noh, J. H.; Yoon, S. C.; Hwang, C. S.; Seok, S. I. *Adv. Mater.* **2015**, *27*, 4013.

(54) Xu, X. B.; Liu, Z. H.; Zuo, Z. X.; Zhang, M.; Zhao, Z. X.; Shen, Y.; Zhou, H. P.; Chen, Q.; Yang, Y.; Wang, M. K. *Nano Lett.* **2015**, *15*, 2402.

(55) García-Valenzuela, J. A.; Baez-Gaxiola, M. R.; Sotelo-Lerma, M. *Thin Solid Films* **2013**, *534*, 126.

(56) Thupakula, U.; Bal, J. K.; Debangshi, A.; Khan, A. H.; Dalui, A.; Acharya, S. *J. Phys. Chem. C* **2012**, *116*, 18564.

(57) Sargent, E. H. *Nat. Photonics* **2009**, *3*, 325.

(58) Nair, G.; Chang, L. Y.; Geyer, S. M.; Bawendi, M. G. *Nano Lett.* **2011**, *11*, 2145.

(59) Knowles, K. E.; Malicki, M.; Weiss, E. A. *J. Am. Chem. Soc.* **2012**, *134*, 12470.

(60) Yu, Y. X.; Zhang, K. X.; Sun, S. Q. *Appl. Surf. Sci*. **2012**, *258*, 7181.

(61) Zhang, N.; Ruan, Y. F.; Ma, Z. Y.; Zhao, W. W.; Xu, J. J.; Chen, H. Y. *Biosens. Bioelectron*. **2016**, *85*, 294.

(62) Zhao, W. W.; Wang, J.; Zhu, Y. C.; Xu, J. J.; Chen, H. Y. *Anal. Chem.* **2015**, *87*, 9520.

(63) Zhang, X. R.; Liu, M. S.; Liu, H. X.; Zhang, S. S. *Biosens. Bioelectron.* **2014**, *56*, 307.

(64) Tanne, J.; Schafer, D.; Khalid, W.; Parak, W. J.; Lisdat, F. *Anal. Chem*. **2011**, *83*, 7778.

(65) Wang, W. J.; Bao, L.; Lei, J. P.; Tu, W. W.; Ju, H. X. *Anal. Chim. Acta* **2012**, *744*, 33.

(66) Xu, Q.; Gu, S. X.; Jin, L. Y.; Zhou, Y. E.; Yang, Z. J.; Wang, W.; Hu, X. Y. *Sensor. Actuat. B-Chem.* **2014**, *190*, 562.

For TOC only

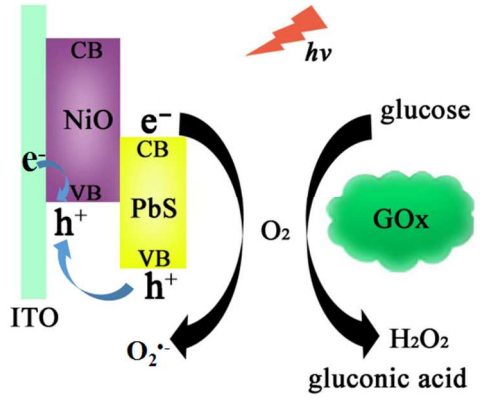
CB
NiO
VB
e⁻
h⁺
ITO
e⁻
CB
PbS
VB
h⁺
hv
O₂
O₂·⁻
glucose
GOx
H₂O₂
gluconic acid